Proceedings of ASME 2019 International Design Engineering Technical Conferences & Computers and Information in Engineering Conference
IDETC/CIE 2019
Aug 18-21, 2019, Anaheim, CA, USA

IDETC2019-97706

DESIGN AND OPTIMIZATION OF AN ORIGAMI-INSPIRED JUMPING MECHANISM WITH NONLINEAR STIFFNESS PROPERTIES

Sahand Sadeghi*, Blake D. Betsill, and Suyi Li
Department of Mechanical Engineering
Clemson University, Clemson, SC, USA

ABSTRACT

This research investigates the feasibility of utilizing origami folding techniques to create an optimized jumping mechanism. As a theoretical example, we study the dynamic characteristics of a jumping mechanism consisting of two masses connected by a Tachi-Miura Polyhedron (TMP) origami structure with nonlinear stiffness characteristics. We show how the desired "strain-softening" effects of the TMP structure can lead to design of jumping mechanisms with optimized performance. The kinematics of TMP origami structure is reviewed and a modified model of its reaction-force displacement curve is presented. We derive the equations of motion of the jumping process and use their numerical solutions extensively for design optimization. Through this process we are able to obtain optimum geometrical configurations for two different objectives: The maximum time spent in the air and the maximum clearance off the ground. Results of this study can lead to emergence of a new generation of more efficient jumping mechanisms with optimized performance in the future.

Keywords*: Jumping mechanism, Origami, Non-linear stiffness, Optimization*

1. INTRODUCTION

Among the myriad of great achievements in human history, invention of robots is a major breakthrough. Robots have affected and revolutionized so many aspects of our mundane life. From industrial [1–3] and military [4] applications to education [5,6] and healthcare [7,8] services, they have been and will continue improving the quality of our lives. Among the various existing categories of robots, mobile robots are particularly important because they can perform tasks that are inaccessible or unsafe for humans [9], such as volcano exploration, coal extraction, and disaster rescue [10]. Mobile robots can be classified into five different categories according to their ground-contact-based modes of locomotion: wheeled robots, tracked robots, snake robots, legged robots, and wheel-legged robots [10]. Among them, the legged robots are particularly advantageous due to their relative superiority in maneuvering and their capability to access vastly different terrains [11] like mountain lands, sands, and even rugged terrains [10].

However, the dynamics of legged robots, in general, is more complicated compared to the wheeled, tracked, or snake robots especially due to their impacts with the ground [12]. They also require complex nonlinear control strategies. Therefore, researchers have been encouraged to study single-legged robotic systems as well [12,13]. Despite the relative simplicity of their configuration, single-legged robots are found to be extremely advantageous in different applications [12]. The locomotion in this kind of robotic systems is achieved by jumping [14], which is a relatively simple mode of locomotion that can be beneficial in terrains that are inaccessible to wheeled or tracked systems [12]. Recently, there have been a surge of interest in single-legged robotic systems and several researchers have studied different facets of jumping mechanisms and their locomotion [15–18].

One of the most important and crucial topics in the field of jumping robots is the energy storage technique. In all of the existent jumping mechanisms, the jumping phase of motion is achieved by an instant release of the stored energy in the system [15]. Therefore, energy storage has an undeniably important role in the performance of the jumping robots [13]. Researchers have proposed various methods for storing energy in robotic systems: From traditional springs [19–21] (compression, extension, or torsional springs), and compressed air [22], to custom-designed elastic elements [23–25]. The latter approach of energy storage essentially uses the nonlinear spring elements to introduce unique and desirable nonlinear dynamic characteristics to jumping robots.

* Address all correspondence to this author: ssadegh@clemson.edu

Nonlinear spring elements have been used in several jumping robots and their effect on the overall dynamic performance has been studied in several researches. For example, in the study by Yamada et al., the snap-through buckling of a closed elastica has been examined as a means of energy storage [25,26]. In another study, Fiorini and Burdick investigated a jumping mechanism with a nonlinear stiffness achieved by implementing a linear spring in a 6-bar geared mechanism [27]. Furthermore, the authors of this paper have recently rigorously examined the effects of using a generic nonlinear spring in a jumping mechanism [13] both numerically and analytically. We showed that utilizing nonlinear springs with "strain-softening" characteristics, can increase the initial stored energy and consequently create higher jumps in terms of center of gravity and ground clearance, while sacrificing only a negligible amount of efficiency [13]. More importantly, results of this study were generic so that they can be applied to different types of nonlinear spring mechanisms. This leads to the research question of this study: Can we use origami structure to materialize the desired nonlinear stiffness characteristics in a jumping mechanism?

Origami – the ancient Japanese art of paper folding – has recently expanded the design and fabrication repertoire of engineers[28]. It has found lots of applications from kinetic architectures [29] and self-folding robots [30] to surgery devices [31] and DNA machines [32]. In addition, researchers have been studying origami folding techniques as a method for achieving tunable nonlinear stiffness recently such as negative and quasi-zero stiffness [28,33–35] and multi-stability [36,37].

Therefore, in this paper, we investigate the feasibility of using origami as the energy storage element in the jumping mechanism and achieve the desired "strain-softening" nonlinear stiffness. To this end, we first analyze the stiffness properties of a re-entrant origami structure based on Tachi-Miura polyhedron (TMP) [38] and investigate the effect of its design parameters on the structure's overall force-displacement relationship. Then, we examine a basic jumping mechanism consisting of two masses connected by the TMP structure—which acts as a nonlinear spring element in the system—and analyze its dynamic jumping behavior. Finally, we try to optimize the design of this origami jumper based on two different performance criteria: 1) jumping air-time and 2) clearance of the bottom mass.

The rest of the paper is organized as follows: In Section 2, we review the governing kinematic relations of TMP structure and its force-displacement curve under quasi-static loading. Furthermore, we modify the mathematical model of its force-displacement curve based on the nonlinear constitutive model of rotational springs proposed by Liu and Paulino [39]. In Section 3, we derive the equations of motion of the jumping mechanism for the pre-jump and post-jump phases of motion. Section 4 focuses on design optimization of the origami structure based on the abovementioned performance criteria. To this end, we solve the derived equations of motion numerically and use the results extensively. Section 5 concludes the paper with a summary and discussion.

2. TACHI-MIURA POLYHEDRON (TMP) BELLOW

In this study, we use a variation of the Tachi-Miura polyhedron (TMP) origami bellow studied by Yasuada and Yang [36] as the basis for our jumping mechanism. The TMP bellow is essentially a linear assembly of identical unit cells and each cell consists of two connected origami sheets (aka. the front sheet and back sheet shown in Figure 1(a,b)). The geometric design of two origami sheets can be uniquely defined based on two fold lines $(l,\ m)$, the side length (d), and a sector angle (α). For clarity, we refer the fold lines that remain parallel to the horizontal *x*-*z* reference plane as the "main-folds" and all other fold lines are the "sub-folds" (Figure 1(b)).

Despite the relatively complex geometry, TMP bellow is *rigid-foldable* in that its folding motion does not induce any deformations in the facets. Therefore, we can assume the facets are rigid, and the fold lines behave like perfect hinges with assigned torsional stiffness. In this way, we can use the virtual work principle and estimate the reaction force F of the TMP bellow along its length direction (*y*-axis in Figure1(a)) as follows[38],

$$F = \frac{-32}{Nd\cos\theta_M}\Big[k_M(N-1)\left(\theta_M-\theta_{M_0}\right)+\ldots \\ Nk_S\left(\theta_S-\theta_{S_0}\right)\frac{\cos^3\theta_G/2\sin\theta_M}{\cos\alpha\sin\theta_S}\Big]. \tag{1}$$

In this equation, N is the number of unit cells in the TMP bellow; k_M and k_S are the equivalent torsional stiffness of the main-folds and sub-folds, respectively; θ_M is the dihedral angle associated with the main-folds, defined between the facets and *x*-*z* reference plane as shown in Figure 1(c); θ_S is the dihedral angle between the facets along the sub-folds; and θ_S is the angle between *x*-axis and a main-fold. Denote u as the change in unit cell height through folding and θ_{M0} as the main fold angle corresponding to the initial, resting configuration, the magnitude of these angles can be calculated as

$$\theta_M = \sin^{-1}\left(\sin\theta_{M0}-\frac{u}{Nd}\right), \tag{2}$$

$$\theta_G = 2\tan^{-1}\left(\tan\alpha\cos\theta_M\right), \tag{3}$$

$$\theta_S = \cos^{-1}\left(\frac{\sin\frac{\theta_G}{2}}{\sin\alpha}\right). \tag{4}$$

Figure 2(a) illustrates the force displacement curve of a TMP bellow design based on $l=m=d=30\text{mm}$, $\alpha=40°$, $\theta_{M0}=65°$, and $k_M=k_S=0.03\,\text{N.m}/rad$. Due to the nonlinear geometric relationships induced by origami folding, the TMP bellow shows a strong nonlinearity. In particular, it shows a

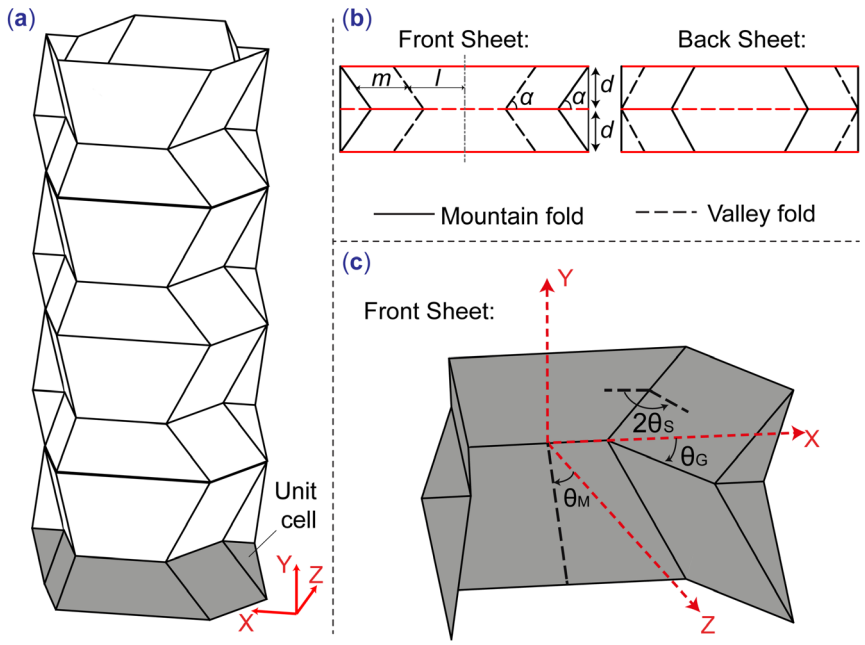

Figure 1: Design of the Tachi-Miura Polyhedron (TMP) bellow. (a) The overall external geometry of a TMP bellow; this one consists of eight unit cells, and one of them is highlighted in gray. (b) The crease design of the front sheet and back sheet that makes up two unit cells. The main-folds are highlighted by red color. (c) The external geometry of a folded front sheet, showing the different angles used in the kinematics and mechanics analysis.

"strain softening" behavior in compression. That is, the TMP exhibits a high stiffness under small compressive deformation, but its stiffness decreases as the deformation increases. Previous study by the authors has shown that such nonlinearity is desired because it can store more energy upon compression compared to the traditional linear spring, leading to a higher jump [13]. Moreover, after careful examinations, we discover that the reaction force generated by the sub-folds shows a stronger nonlinearity than the main-folds. Therefore, we will intentionally weaken main-folds and stiffen up the sub-folds to strengthen the desired non-linearity. This allows us to neglect the contribution of the main-folds to the overall reaction force, and simplify equation (1) into the following:

$$F = \frac{-32k_S}{Nd\cos\theta_M}\left[N\left(\theta_S-\theta_{S0}\right)\frac{\cos^3\frac{\theta_G}{2}\sin\theta_M}{\cos\alpha\sin\theta_S}\right]. \tag{5}$$

However, this reaction force equation does not consider the deformation limits due to rigid folding. That is, TMP bellow can only be folded in-between its compression limit at $\theta_S = 0°$ (fully compressed) and extension limit at $\theta_S = 90°$ (fully stretched). However, in reality when the TMP is compressed near $\theta_S = 0°$, its facets would come into contact with each other and resist further compression. On the other hand, when the TMP is extended near $\theta_S = 90°$, both the front and back sheets are stretched flat so that the overall tension stiffness would increase significantly. To incorporate these deformation limits by folding, we adopt the method developed by Liu and Paulino [37] and set two folding angle limits: $\theta_1 = 20°$ for compression and $\theta_2 = 70°$ for tension. When $\theta_S < \theta_1$, the reaction force equation (5) is modified into the following:

$$F = \frac{-32k_S}{Nd\cos\theta_M}[N(\theta_1-\theta_{S0})+\ldots \\ \frac{2\theta_1}{\pi}\tan\left(\frac{\pi(\theta_S-\theta_1)}{2\theta_1}\right)\frac{\cos^3\frac{\theta_G}{2}\sin\theta_M}{\cos\alpha\sin\theta_S}]. \tag{6}$$

Similarly, when $\theta_S > \theta_2$, the reaction force becomes,

$$F = \frac{-32k_S}{Nd\cos\theta_M}[N(\theta_2-\theta_{S_0})+\ldots \\ \frac{2\theta_2}{\pi}\tan(\frac{\pi(\theta_S-\theta_2)}{2\theta_2})\frac{\cos^3\frac{\theta_G}{2}\cos\theta_M}{\cos\alpha\cos\theta_S}] \tag{7}$$

Figure 2(b) illustrate the modified reaction force, which is used for the subsequent dynamic analysis and optimization.

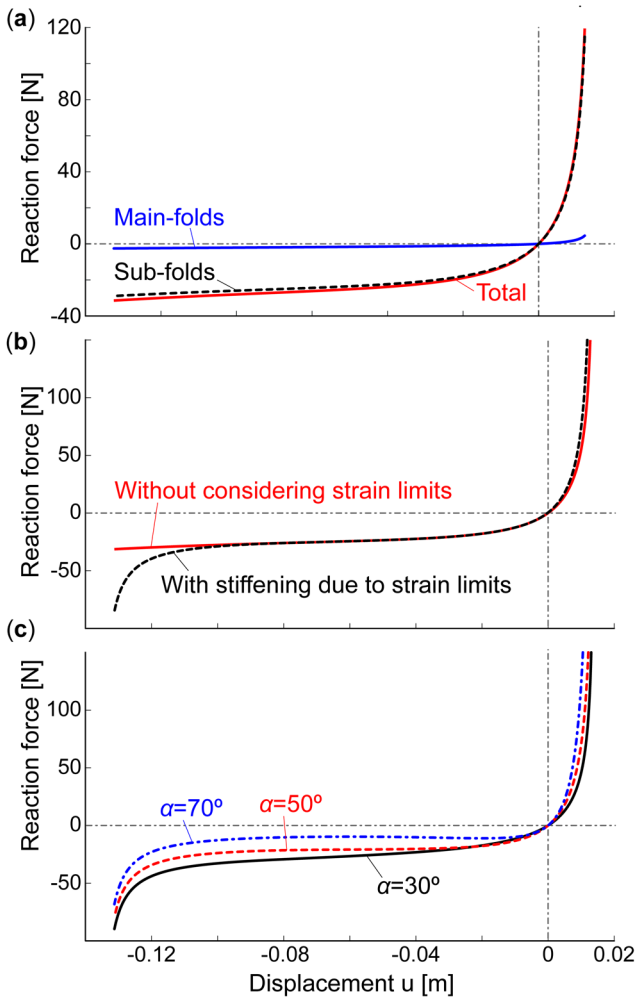

Figure 2: The force-displacement curve of a TMP bellow. (**a**) The contribution of main-folds and sub-folds to the overall reaction force, and the sub-folds show the desired "strain softening" behavior in compression. (**b**) The modified reaction force curve considering the deformation limit due to folding. (**c**) The reaction force curve corresponding to different α angles, while all other design variables remain the same as those used in (a).

Figure 2(c) illustrates the effect of the sector angle α on the force-displacement curve. When other design variables are fixed, increasing the α angle would decrease the reaction force in the structure when compressed. This leads to less stored strain energy. For this reason we would expect smaller alpha angles to lead to better jumping performance.

3. The Dynamics of TMP Jumper

The TMP jumping mechanism (shown in Figure 3) consists of two identical masses connected by a TMP bellow, which serves as the energy storage element in the mechanism. It is worth noting again that the TMP exhibits nonlinear stiffness properties. In order to only focus on the effects of nonlinear stiffness on the jumping performance of the origami structure, in this study, we assume that damping is zero. One should notice although this

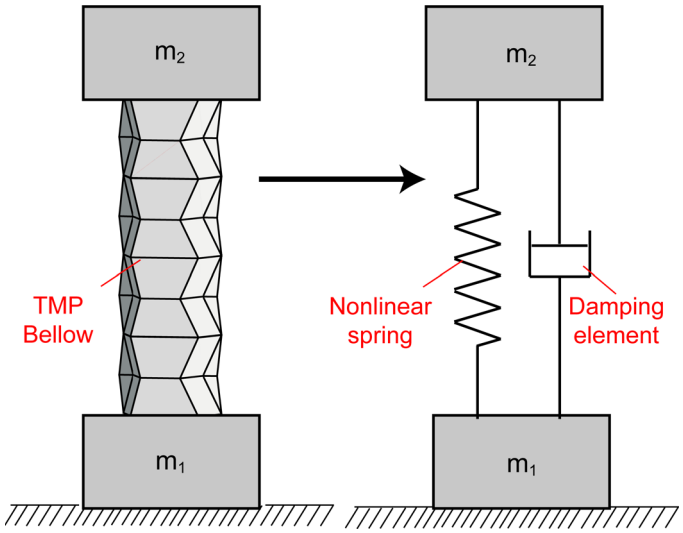

Figure 3: The jumping mechanism based on TMP bellow and its equivalent system. Here the nonlinear spring shows the force-displacement curves defined in equations (5-7).

might affect the dynamics quantitatively, it does not alter the qualitative behavior of the structure, as long as it exhibits monostable hardening characteristics. To initiate jumping, this mechanism is actuated via an external force acting on the upper mass, which deforms the TMP bellow and thus stores energy in the system.

The dynamics of jumping can be divided into two distinct phases: 1) pre-jump phase and 2) post-jump phase. To focus on the effects of the TMP bellow on the dynamic performance of the jumping mechanism, we assumed that the masses are equal: $m_1 = m_2 = M$. In the following two subsections we investigate the motion in these two phases and derive the equations of motion for pre-jump and post-jump phases, respectively.

3.1 Pre-Jump Phase

In this phase, the jumping mechanism is actuated by an external force on the upper mass, which moves it to a certain initial displacement (d). Then the external force is removed and the reaction force from TMP bellow accelerates the upper mass upward. This pre-jump phase of motion continues until the bottom mass leaving the ground. One can derive the governing equation of motion for this phase as:

$$M\ddot{Y}_2 = -F(Y_2 - l_0) - Mg, \tag{8}$$

where M is the mass of the upper body; $F(Y_2 - l_0)$ is the reaction force of the TMP bellow defined in equation (5); l_0 is the initial, resting length of the TMP; $\ddot{Y}_2$ and Y_2 are the acceleration and position of the upper mass (relative to the ground), respectively.

3.2 Post-Jump Phase

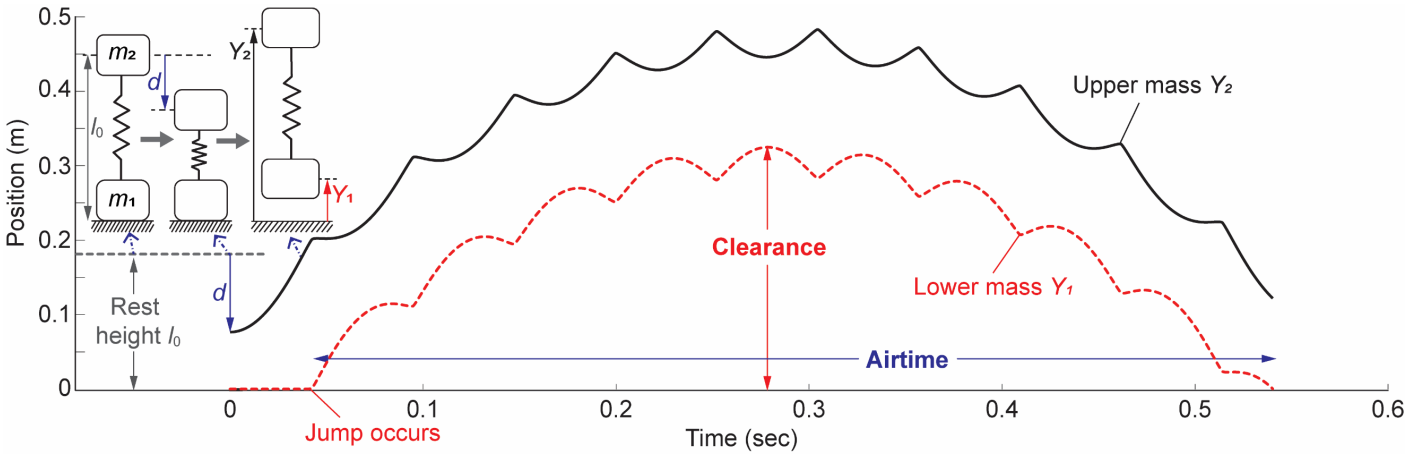

Figure 4: A typical time response of the TMP origami jumper. The schematic plots at the upper left corner illustrates the origami jumper at resting configuration, initial configuration when the upper mass is compressed, and post jump phase, respectively. The two objective functions of the design optimization: Airtime and Clearance are highlighted. Notice the internal oscillation during the post jump phase influences the Clearance performance.

If the jumping mechanism can overcome the gravitational force after the deformation of the TMP bellow becomes positive, the jump can occur. In other words, once the restoring force of the TMP bellow on the lower mass exceeds its weight (aka. $F(Y_{2,jump} - l_0) \geq Mg$), the jumping mechanism enters the second phase of motion. Here $Y_{2,jump}$ stands for the critical upper mass displacement when the jump occurs.

Once the bottom mass has left the ground, the governing system of coupled equations of motion can be described as:

$$\begin{aligned} M\ddot{Y}_1 &= F(Y_2 - Y_1 - l_0) - Mg, \\ M\ddot{Y}_2 &= -F(Y_2 - Y_1 - l_0) - Mg. \end{aligned} \tag{9}$$

The initial conditions of equation (9) can be extracted from the solution of the pre-jump phase equation (8). Figure 5 shows a typical time response of an origami jumper, in which one can clearly identify the two different phases of jumping. Moreover, once the origami jumper is airborne, it also exhibits an internal oscillation with respect to its center of mass. In the next section, we use the numerical solution of equation (8) and (9) to optimize the performance of the jumping mechanism.

4. TMP Design Optimization

The goal of this optimization is to identify the TMP bellow design that can lead to the best jumping performance. To this end, we describe the jumping performance based on two different objectives: Airtime and Clearance (illustrated in Figure 4). Airtime is the total time that the jumping mechanism spends in the air; and Clearance is the peak height achieved by the lower mass. We normalize the Clearance by the rest height of TMP bellow and use the normalized values as the optimization objective function.

There are five design variables that that can be tailored to optimize the jumping performance. The definition and range of these variables are listed in Table 1, and Figure 1 illustrates how they relate to the overall geometry of TMP bellow. Moreover, three geometric constraints are imposed. The first constraint ensures that the design of TMP bellow is properly defined and there are no conflicting crease lines. The second constraint defines a minimum main-fold length for the ease of manufacturing and assembly. The third constraint sets an upper limit on the unit cell length. The additional 15mm in the third constraint is for an extended tab to facilitate the assembly of two sheets.

Table 1. The design variables and geometric constraints used in the design optimization.

N : Unit cell #	$4 \leq N \leq 10$
d : Side length	$20\text{mm} \leq d \leq 40\text{mm}$
α : Sector angle	$30^\circ \leq \alpha \leq 70^\circ$
l : Fold length	$20\text{mm} \leq l \leq 40\text{mm}$
m : Fold length	$20\text{mm} \leq m \leq 40\text{mm}$
Constraint 1:	$2l - d\cot\alpha + 2m\cos\alpha \geq 0$
Constraint 2:	$\frac{d}{2\tan\alpha} - l \leq -10\text{mm}$
Constraint 3:	$2\left(l + m + \frac{d}{2}\tan\left(\frac{\pi}{2} - \alpha\right) + 15\right) \leq 300\text{mm}$

In this study, the three constraints on design variables are defined based on the fabrication capabilities available to the authors. Increasing the variables beyond the upper limits would

require additional fabrication equipment; while reducing them below the lower limit would makes assembly too difficult. Regardless, we can still obtain valuable insights on the correlations between the design variables and jumping performance within these constraints.

Table 2. Other design variables used in the optimization.

M : End masses	$m_1 = m_2 = M = 0.25\text{kg}$
θ_{M_0} : Resting main-fold angle	$\theta_{M_0} = 65^\circ$
FR : Initial folding ratio	$FR = \frac{90^\circ - \theta_M}{90^\circ} \times 100\% = 75\%$
k_S : Sub-fold stiffness	$k_S = 0.0383\, N.m/rad$

Besides the geometric design variables of TMP bellow, the magnitudes of some other variables are defined for the optimization (Table 2). One of them is the stress-free, resting folding angle of the main-folds θ_{M0}. However, a very large resting folding angle is difficult to achieve in experiments. Based on repeated trial-and-errors using TMP prototypes of different geometric designs, $\theta_{M0} = 65^\circ$ is found to be a realistic value. Another important variable is the initial folding ratio, which is essentially the initial condition of the dynamic simulation discussed below. Again, after repeated trial-and-error, it is found that an initial folding ratio of 75% is preferred because it can achieve the maximum stored energy for jumping without inducing any significant plastic deformation. The crease torsional stiffness coefficient k is estimated based on the experimental data gathered from different shim stock, which will be used to stiffen the sub-folds.

We numerically simulate the jumping behavior of the TMP mechanism in MATLAB using ode45 solver for the different jumping phases outlined in Section 3. In these simulations, we assume the upper mass is lowered so that the TMP bellow is compressed to the initial folding ratio of 75%, and then the upper mass is released for jumping. We then use the ode45 solver to obtain the pre-jump time response according to equation (8). Based on this response, we can identify the moment when the TMP bellow is stretched to the point that its resulting tension force surpass the weight of lower mass. At this moment, the lower mass leaves the ground so that we can use this as the initial conditions for the post-jump phase. Ode45 solver is used again to obtain the time response of the jumping phase so that the Airtime and Clearance can be recorded.

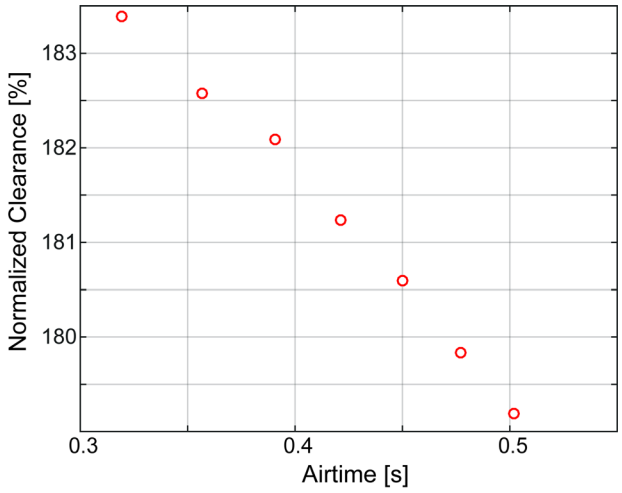

Figure 5: Pareto front obtained in the optimization results.

To optimize the TMP bellow design, we integrate the jumping simulations and ModeFrontier using the NSGA-II optimization algorithm. NSGA-II is a common genetic algorithm for multi-objective optimization problems. We use a total population size of 2500 individuals across 5 generations. Interested readers can refer to [40] for a complete description of this optimization method. The optimization results according to each objective function are represented in Table 3.

From the results in Table 3, one can observe that the optimized sector angle α is always at its lower limit. As we explained in Section 2, a lower α angle corresponds to a stronger nonlinearity in the force-displacement relationship of the TMP bellow (Figure 2(c)), which is desired for better jumping performance. The optimized unit cell side length d and the crease length l, m are the same. Moreover, d and m are also at their lower limit. The unit-cell side length d appears in the denominator of the reaction force equation (9), so a small side length corresponds to a bigger reaction force and therefore more stored strain energy for jumping. The crease length m does not appear in the reaction force equation explicitly, but its value is kept low to avoid violating the third geometric constraint. Similarly, the value of crease length l is also kept low to avoid violating the second geometric constraint.

The difference between the two optimized designs are the number of unit cells N. More unit cells in a TMP bellow means a larger initial displacement of the upper mass, therefore more

Table 3. Optimized TMP bellow designs for Airtime and Clearance Objectives

	N	***α*** [°]	***d*** [mm]	***l*** [mm]	***m*** [mm]	**Airtime** [sec]	**Normalized Clearance**
Airtime Optimum	10	30	20	28.5	20	0.502	179%
Clearance Optimum	4	30	20	28.5	20	0.320	183%

strain energy is stored for jumping and a longer airtime. However, increasing the N values also increases overall structure height, which can negate the performance of normalized Clearance. Such a trade-off between Airtime and Clearance can be illustrated in the pareto front shown in Figure 5.

5. Conclusion and Discussion

In this study we investigate the idea of utilizing origami folding techniques to enhnace the performance of a jumping mechanism. We study the feasibility of using Tachi-Miura Polyhedron (TMP) origmai struture as the energy storing unit in a mechanism consisting of two masses, through analyzing the dynamic characteristics of the system. The TMP origami structure exhibits nonlinear stiffness characteristics. We show how the desired "strain-softening" effects of the TMP structure can lead to design of jumping mechanisms with optimized performance. We present a review of the kinematics of TMP origami structure and derive a modified model of its reaction force-displacement curve. We derive the equations of motion of the jumping process and use their numerical solutions extensively for design optimization. The optimum geometric configurations for two different objectives are derived: The maximum time spent in the air (a.k.a airtime) and the maximum clearance off the ground. Although this study has been conducted on a specific origami pattern (TMP bellow), the results show that origami folding techniques can add more tools to the repertoire of robotic researchers to create jumping mechansisms with higher performance. Therefore, the outcome of this research can lead to emergence of a new generation of more efficient jumping mechanisms with optimized performance in the future.

Acknowledgment

The authors acknowledge the support from the National Science Foundation (Award # CMMI-1633952, 1751449 CAREER) and Clemson University (via startup funding and the CECAS Dean's Faculty Fellow Award).

References

[1] Chua, P. Y., Ilschner, T., and Caldwell, D. G., 2003, "Robotic Manipulation of Food Products - A Review," Ind. Rob., **30**(4), pp. 345–354.

[2] Shukla, A., and Karki, H., 2016, "Application of Robotics in Onshore Oil and Gas Industry-A Review Part I," Rob. Auton. Syst., **75**, pp. 490–507.

[3] Bogue, R., 2011, "Robots in the Nuclear Industry: A Review of Technologies and Applications," Ind. Rob., **38**(2), pp. 113–118.

[4] Reddy, A. H., Kalyan, B., and Murthy, C. S. N., 2015, "Mine Rescue Robot System – A Review," Procedia Earth Planet. Sci., **11**, pp. 457–462.

[5] Benitti, F. B. V., 2012, "Exploring the Educational Potential of Robotics in Schools: A Systematic Review," Comput. Educ., **58**(3), pp. 978–988.

[6] Belpaeme, T., Kennedy, J., Ramachandran, A., Scassellati, B., and Tanaka, F., 2018, "Social Robots for Education: A Review," Sci. Robot., **3**(21), p. eaat5954.

[7] Jamwal, P. K., Hussain, S., and Xie, S. Q., 2015, "Review on Design and Control Aspects of Ankle Rehabilitation Robots," Disabil. Rehabil. Assist. Technol., **10**(2), pp. 93–101.

[8] Robinson, H., MacDonald, B., and Broadbent, E., 2014, "The Role of Healthcare Robots for Older People at Home: A Review," Int. J. Soc. Robot., **6**(4), pp. 575–591.

[9] Liu, J., Tan, M., and Zhao, X., 2007, "Legged Robots — an Overview," Trans. Inst. Meas. Control, **29**(2), pp. 185–202.

[10] Zhuang, H., Gao, H., Deng, Z., Ding, L., and Liu, Z., 2014, "A Review of Heavy-Duty Legged Robots," Sci. China Technol. Sci., **57**(2), pp. 298–314.

[11] Dubey, S., Prateek, M., and Saxena, M., 2015, "Robot Locomotion – A Review," Int. J. Appl. Eng. Res., **10**(3), pp. 7357–7369.

[12] Sayyad, A., Seth, B., and Seshu, P., 2007, "Single-Legged Hopping Robotics Research - A Review," Robotica, **25**(5), pp. 587–613.

[13] Sadeghi, S., Betsill, B. D., Tallapragada, P., and Li, S., 2018, "The Effect of Nonlinear Springs in Jumping Mechanisms," *Volume 1: Advances in Control Design Methods; Advances in Nonlinear Control; Advances in Robotics; Assistive and Rehabilitation Robotics; Automotive Dynamics and Emerging Powertrain Technologies; Automotive Systems; Bio Engineering Applications; Bio-Mecha*, ASME, p. V001T04A002.

[14] Bergbreiter, S. E., 2007, "Autonomous Jumping Microrobots," ProQuest Diss. Theses, **3306062**, p. 150.

[15] Zhao, J., Xu, J., Gao, B., Xi, N., Cintron, F. J., Mutka, M. W., and Xiao, L., 2013, "MSU Jumper: A Single-Motor-Actuated Miniature Steerable Jumping Robot," IEEE Trans. Robot., **29**(3), pp. 602–614.

[16] Haldane, D. W., Plecnik, M. M., Yim, J. K., and Fearing, R. S., 2016, "Robotic Vertical Jumping Agility via Series-Elastic Power Modulation," Sci. Robot., **1**(1), p. eaag2048.

[17] Schammass, A., Caurin, G. A. P., and Valente, C. M. O., 2001, "Control of a One-Legged Robot with Energy Savings," J. Brazilian Soc. Mech. Sci., **23**(1), pp. 41–48.

[18] Albro, J., and Bobrow, J., 2001, "Optimal Motion Primitives for a 5 Dof Experimental Hopper," Robot. Autom. 2001. …, pp. 3630–3635.

[19] Zhang, J., Song, G., Qiao, G., Meng, T., and Sun, H., 2011, "An Indoor Security System with a Jumping Robot as the Surveillance Terminal," IEEE Trans. Consum. Electron., **57**(4), pp. 1774–1781.

[20] Scarfogliero, U., Stefanini, C., and Dario, P., 2009, "The Use of Compliant Joints and Elastic Energy Storage in Bio-Inspired Legged Robots," Mech. Mach. Theory, **44**(3), pp. 580–590.

[21] Zhao, J., Xi, N., Gao, B., Mutka, M. W., and Xiao, L., 2010, "Design and Testing of a Controllable Miniature Jumping Robot," IEEE/RSJ 2010 Int. Conf. Intell.

Robot. Syst. IROS 2010 - Conf. Proc., (November), pp. 3346–3351.

[22] Tsukagoshi, H., Sasaki, M., Kitagawa, A., and Tanaka, T., 2005, "Design of a Higher Jumping Rescue Robot with the Optimized Pneumatic Drive," Proc. - IEEE Int. Conf. Robot. Autom., **2005**(April), pp. 1276–1283.

[23] Kesner, S., Plante, J., Dubowsky, S., and Boston, P., 2007, "A Hopping Mobility Concept for a Rough Terrain Search and Rescue Robot," Adv. Climbing Walk. Robot. Proc., pp. 271–280.

[24] Dubowsky, S., Kesner, S., Plante, J., and Boston, P., 2008, "Hopping Mobility Concept for Search and Rescue Robots," Ind. Robot An Int. J., **35**(3), pp. 238–245.

[25] Yamada, A., Watari, M., Mochiyama, H., and Fujimoto, H., 2008, "An Asymmetric Robotic Catapult Based on the Closed Elastica for Jumping Robot," pp. 232–237.

[26] Yamada, A., Mameda, H., Mochiyama, H., and Fujimoto, H., 2010, "A Compact Jumping Robot Utilizing Snap-through Buckling with Bend and Twist," IEEE/RSJ 2010 Int. Conf. Intell. Robot. Syst. IROS 2010 - Conf. Proc., pp. 389–394.

[27] Fiorini, P., and Burdick, J., 2003, "The Development of Hopping Capabilities for Small Robots," Auton. Robots, **14**(2–3), pp. 239–254.

[28] Li, S., Fang, H., Sadeghi, S., Bhovad, P., and Wang, K.-W., 2019, "Architected Origami Materials: How Folding Creates Sophisticated Mechanical Properties," Adv. Mater., **31**(5), p. 1805282.

[29] Filipov, E. T., Tachi, T., and Paulino, G. H., 2015, "Origami Tubes Assembled into Stiff, yet Reconfigurable Structures and Metamaterials," Proc. Natl. Acad. Sci., **112**(40), pp. 12321–12326.

[30] Felton, S., Tolley, M., Demaine, E., Rus, D., and Wood, R., 2014, "A Method for Building Self-Folding Machines," Science, **345**(6197), pp. 644–646.

[31] Johnson, M., Chen, Y., Hovet, S., Xu, S., Wood, B., Ren, H., Tokuda, J., and Tse, Z. T. H., 2017, "Fabricating Biomedical Origami: A State-of-the-Art Review," Int. J. Comput. Assist. Radiol. Surg.

[32] Wang, P., Meyer, T. A., Pan, V., Dutta, P. K., and Ke, Y., 2017, "The Beauty and Utility of DNA Origami," Chem, **2**(3), pp. 359–382.

[33] Fang, H., Li, S., and Wang, K. W., 2016, "Self-Locking Degree-4 Vertex Origami Structures," Proc. R. Soc. A Math. Phys. Eng. Sci., **472**(2195), p. 20160682.

[34] Sadeghi, S., and Li, S., 2019, "Fluidic Origami Cellular Structure with Asymmetric Quasi-Zero Stiffness for Low-Frequency Vibration Isolation," Smart Mater. Struct., **28**(6), p. 065006.

[35] Sadeghi, S., and Li, S., 2017, "Harnessing the Quasi-Zero Stiffness From Fluidic Origami for Low Frequency Vibration Isolation," *Volume 2: Modeling, Simulation and Control of Adaptive Systems; Integrated System Design and Implementation; Structural Health Monitoring*, ASME, p. V002T03A008.

[36] Fang, H., Li, S., Ji, H., and Wang, K. W., 2017, "Dynamics of a Bistable Miura-Origami Structure," Phys. Rev. E, **95**(5), p. 052211.

[37] Sadeghi, S., and Li, S., 2019, "Analyzing the Bi-Directional Dynamic Morphing of a Bi-Stable Water-Bomb Base Origami," *Behavior and Mechanics of Multifunctional Materials XIII*, H.E. Naguib, ed., SPIE, p. 27.

[38] Yasuda, H., and Yang, J., 2015, "Reentrant Origami-Based Metamaterials with Negative Poisson's Ratio and Bistability," Phys. Rev. Lett., **114**(18), pp. 1–5.

[39] Liu, K., and Paulino, G. H., 2017, "Nonlinear Mechanics of Non-Rigid Origami: An Efficient Computational Approach," Proc. R. Soc. A Math. Phys. Eng. Sci., **473**(2206), p. 20170348.

[40] Deb, K., Pratap, A., Agarwal, S., and Meyarivan, T., 2002, "A Fast and Elitist Multiobjective Genetic Algorithm NSGA-II" *IEEE Transactions on Evolutionary Computation,* vol. 6, pp 182-197